

Supporting information

**The overlooked role of reduced graphene oxide in the reinforcement of hydrophilic polymers**

A. Flores, H. J. Salavagione, F. Ania, G. Martínez, G. Ellis, M. A. Gómez-Fatou

**Experimental**

*Materials*

PVA was purchased from Aldrich (99+% hydrolyzed,  $M_w \approx 89000-98000$  g/mol). Graphite oxide was prepared by oxidation of graphite powder (Aldrich, 99.99 %, particle size 45  $\mu\text{m}$ ) according to the Hummer's method.<sup>1</sup>

*Covalent GO-PVA.* The esterification was carried out following a previously reported approach.<sup>2</sup> Briefly, 40 mg of graphite oxide and 0.4 g of PVA (9 mmol equivalent to OH group) were suspended in DMSO (20 mL) and the suspension was gently stirred and maintained at 70 °C under nitrogen for 3 days. Then, a solution of N-N-dicyclohexylcarbodiimide (DCC) (1.85 g, 9 mmol) and 4-dimethylaminopyridine (DMAP) (0.135 g, 1.1 mmol) in DMSO (20 mL) were added, and the resulting mixture was stirred at room temperature for 3 days. The coagulation of the polymer nanocomposite was accomplished by adding the suspension into 100 mL of methanol under vigorous stirring. The solid GO-PVA was filtered, washed with methanol and dried at 50 °C under vacuum. In order to eliminate rest of non-reacted GO, the nanocomposites were re-dissolved in hot water, centrifuged at a high speed (12,000 rpm) and the dark-colored supernatant solution was coagulated with methanol. This procedure was repeated twice. The final composition of the product was determined from <sup>1</sup>H NMR experiments in DMSO-*d*<sub>6</sub> by integration of the signal corresponding to

hydroxyl protons next to acetate groups in esterified PVA.<sup>2,3</sup> Within the experimental uncertainties, the degree of functionalization was around 1.8%.

*Covalent RGO-PVA.* For the reduction of GO in GO-PVA, 50 mg of GO-PVA was dissolved in 20 mL hot water and the temperature of the solution was left to cool to room temperature. Then, 2 mL of hydrazine were added and the mixture was maintained under magnetic stirring at room temperature for 72 h. The product was coagulated in 100 mL methanol, filtered and washed with abundant methanol. Oxidative debris commonly appears complexed to oxygen functionalized graphene sheets.<sup>4</sup> This can significantly alter the noncovalent absorption of molecules.<sup>5</sup> However, it has been suggested that reduction of GO with hydrazine removes oxidation debris.<sup>6</sup> In agreement with the latter contention, Figure S1 illustrates the Thermogravimetric Analysis (TGA) of a RGO-PVA sample showing that debris is not present in the final material.

PVA, GO-PVA and RGO-PVA films ~ 200  $\mu\text{m}$  thick were prepared by casting and evaporation from 50 mg mL<sup>-1</sup> aqueous solution. X-ray diffraction measurements taken at RH = 31% reveal similar degrees of crystallinity,  $X_c$ , for the three samples:  $X_c = 0.39$ , 0.38 and 0.36 for PVA, RGO-PVA and GO-PVA respectively (see Fig. S8).

#### *Thermogravimetric analysis*

The thermogravimetric analysis was performed in a Q500 TGA from (TA Instruments). The samples were dried under dynamic vacuum prior to the experiments and then placed in a platinum pan. The loss of weight was monitored from room temperature to 800 °C at a heating rate of 10 °C min<sup>-1</sup>, under nitrogen atmosphere.

#### *Water absorption measurements*

The amount of absorbed water at different humidity conditions was measured by gravimetry in a Mettler Toledo microbalance (sensitivity =  $10^{-5}$  g) on PVA and RGO-PVA films of similar dimensions. The films were initially dried under vacuum at 80 °C and then introduced into a desiccator with controlled RH for 3 h before weighing.

#### *Contact angle measurements*

Contact angles were measured at 25 °C with Milli-Q grade water by the sessile drop method using a conventional drop shape analysis technique (Attension Theta optical tensiometer).

#### *Nanoindentation tests*

Films ( $10 \times 5$  mm<sup>2</sup>) were placed vertically in a plastic holding clip and embedded in an epoxy resin (Epofix). The top surface of the resin was dry polished with grinding papers of progressively smaller grain size up to P4000 silicon carbide paper and finished with a Buehler micro-cloth, to expose the cross-section area. Nanoindentation tests were performed using a Nanoindenter G200 (Agilent Tech.) with the continuous stiffness measurement (CSM) technique.<sup>7,8</sup> During the loading cycle, the load was incremented at a constant  $\dot{P}/P$  ratio in order to ensure a constant indentation strain rate during the loading cycle. A sinusoidal force of 2 nm of amplitude and 45 Hz of frequency was superimposed to the quasi-static load during the loading. The indenter displacement is phase-shifted with respect to the excitation force. The contact stiffness can be calculated at any point during the loading portion. In turn,  $H$  and  $E'$  can be derived following:<sup>9-15</sup>

$$\frac{E'}{1-\nu^2} = \frac{\sqrt{\pi}}{2} \frac{1}{\beta\sqrt{A_c}} S \quad (1)$$

$$H = \frac{P}{A_c} \quad (2)$$

Where  $\nu$  is Poisson's ratio of the material, taken to be 0.35 in all cases,  $\beta$  is a geometric factor (we take  $\beta = 1.034$  for a Berkovich indenter) and  $A_c$  is the contact area at an applied load  $P$ . The area function describing  $A_c$  was calculated as a function of the contact penetration depth,  $h_c$ , using a fused silica standard. On the other hand,  $h_c$  was estimated using  $h_c = h - 0.75 P/S$  where  $h$  is the total penetration depth. A polycarbonate (PC) standard plate (Advanced Surface Mechanics, ASMEC GmbH) was employed to validate the  $E'$  values obtained with our instrumentation. The standard manufacturer provided  $E' = 2.8$  GPa, determined using instrumented indentation, a value which is in close agreement with that obtained in our laboratory,  $E' = 2.86 \pm 0.01$  GPa for  $h > 500$  nm.

#### *Scanning electron microscopy (SEM) studies*

The surfaces of the films used for nanoindentation tests were examined using a SU8000 Hitachi scanning electron microscope available in the Characterization Service of the Institute of Polymer Science & Technology (see Fig. S2). Samples were not metal coated prior to imaging. Fig. S2 reveals limited surface roughness for PVA and RGO-PVA although some protuberances, arising most likely from the polishing process, can be discerned. This is indeed in agreement with the indentations studies that reveal constant mechanical properties for indentation penetration depths above 500 nm.

## Results.

Table S1. Values for the water uptake at different RH and contact angles of a drop of water on the surface of the samples studied in this work.

<i>Water uptake / mol<sub>H<sub>2</sub>O</sub>.cm<sup>-3</sup></i>		
RH %	PVA	RGO-PVA
35	6.8 x 10 <sup>-3</sup>	3.4 x 10 <sup>-3</sup>
55	9.8 x 10 <sup>-3</sup>	4.5 x 10 <sup>-3</sup>

<i>Surface response to water</i>		
Water contact angle	Not measurable (very low)	62°

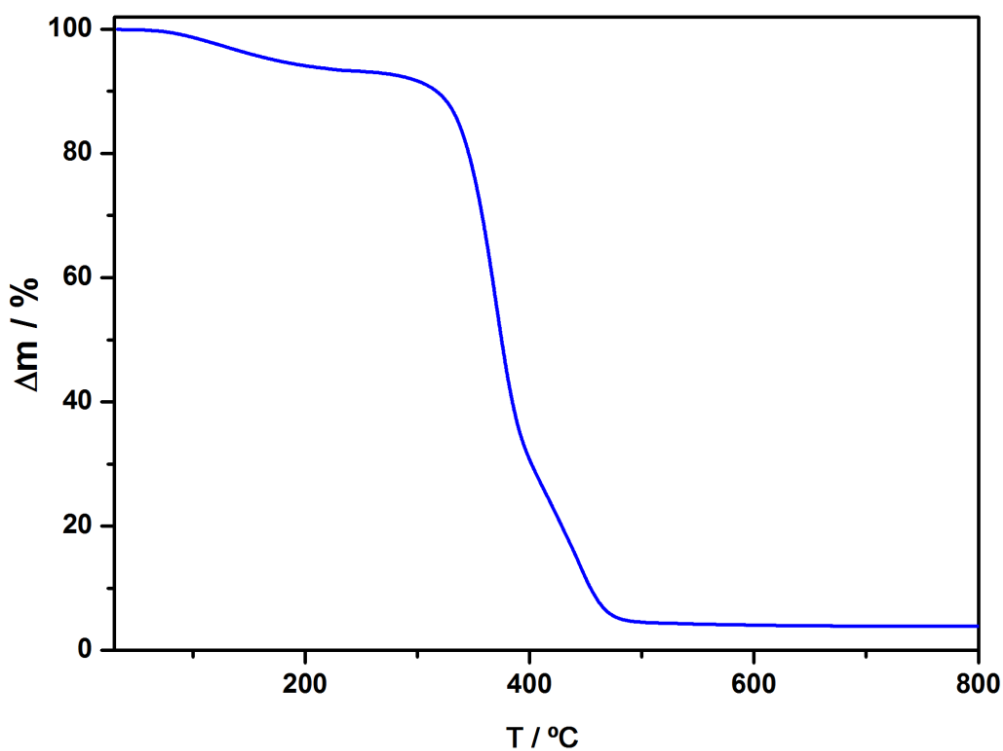


Fig S1. Thermogravimetric curve from a RGO-PVA film.

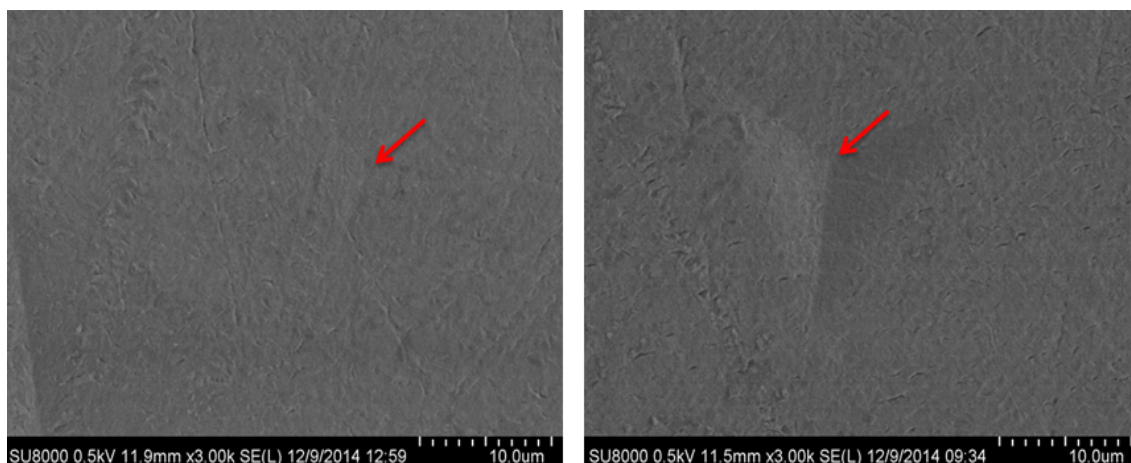


Fig. S2. SEM images of the surfaces used for indentation studies: (left) PVA, (right) RGO-PVA. The residual impressions produced using a Berkovitch indenter can be distinguished. Arrows indicate the location of the initial contact.

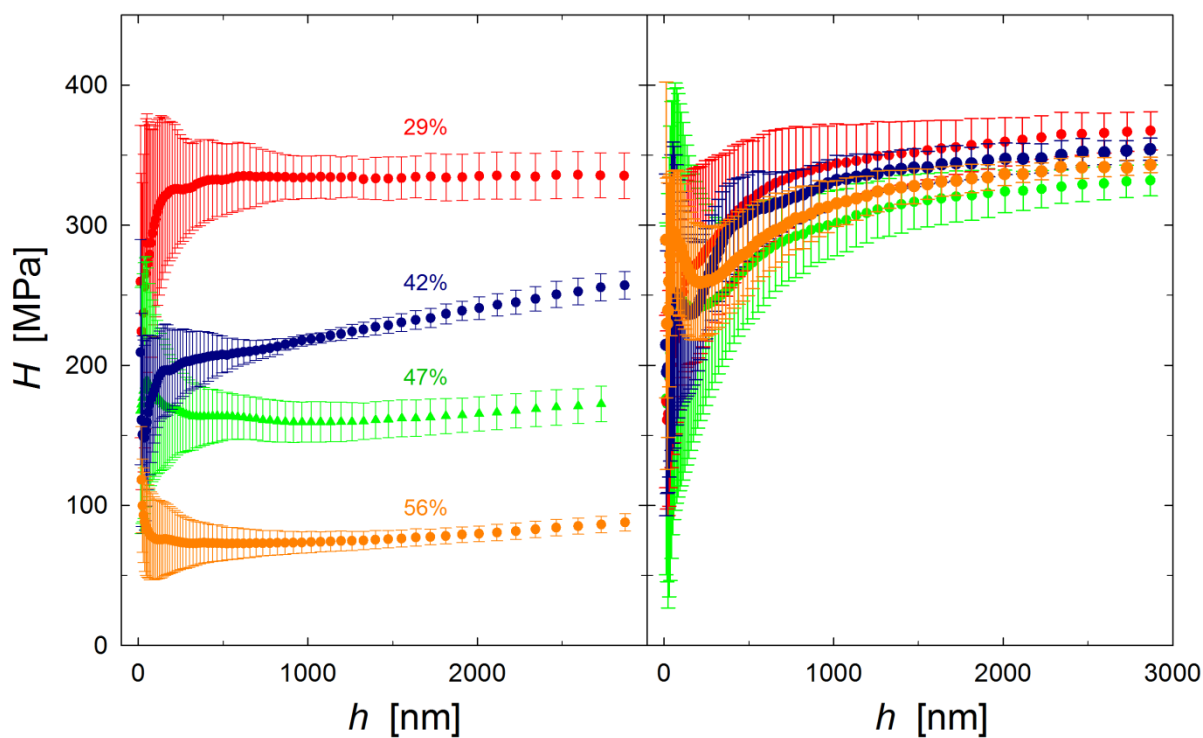


Fig. S3. Hardness,  $H$ , as a function of displacement into the surface,  $h$ , at different chamber RH for: (left) PVA and (right) RGO-PVA.  $\dot{\varepsilon} = 0.05 \text{ s}^{-1}$ .

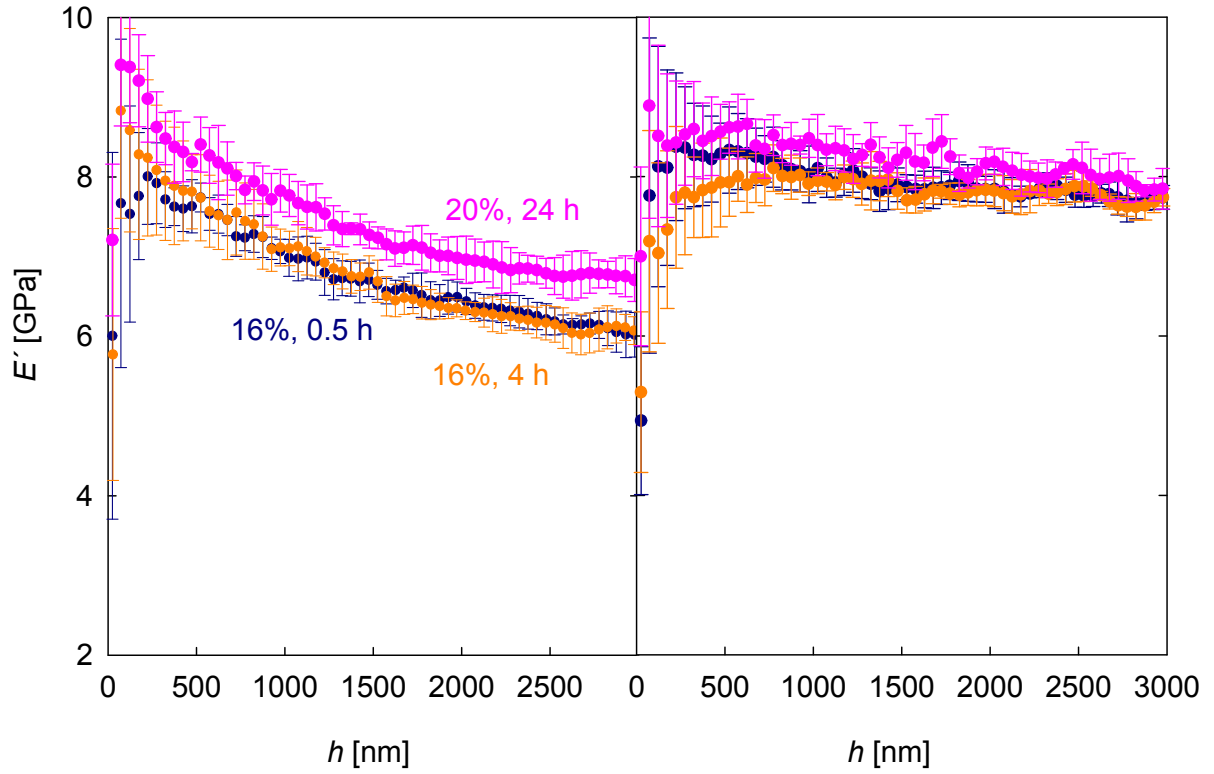


Fig. S4. Storage modulus as a function of indenter displacement for (left) PVA and (right) RGO-PVA conditioned at low humidity environment. The moisture level inside the nanoindentation chamber was achieved by introducing  $P_2O_5$  powder. This procedure allowed stabilizing the RH in the chamber at a value of 16% for a few hours. After 24 h, the RH in the nanoindenter cabinet had raised to 20% as indicated in the figure. Prior to indentation measurements, samples were stored for 10 days at ambient conditions of RH = 35 - 45%.  $\dot{\epsilon} = 0.05 \text{ s}^{-1}$ .

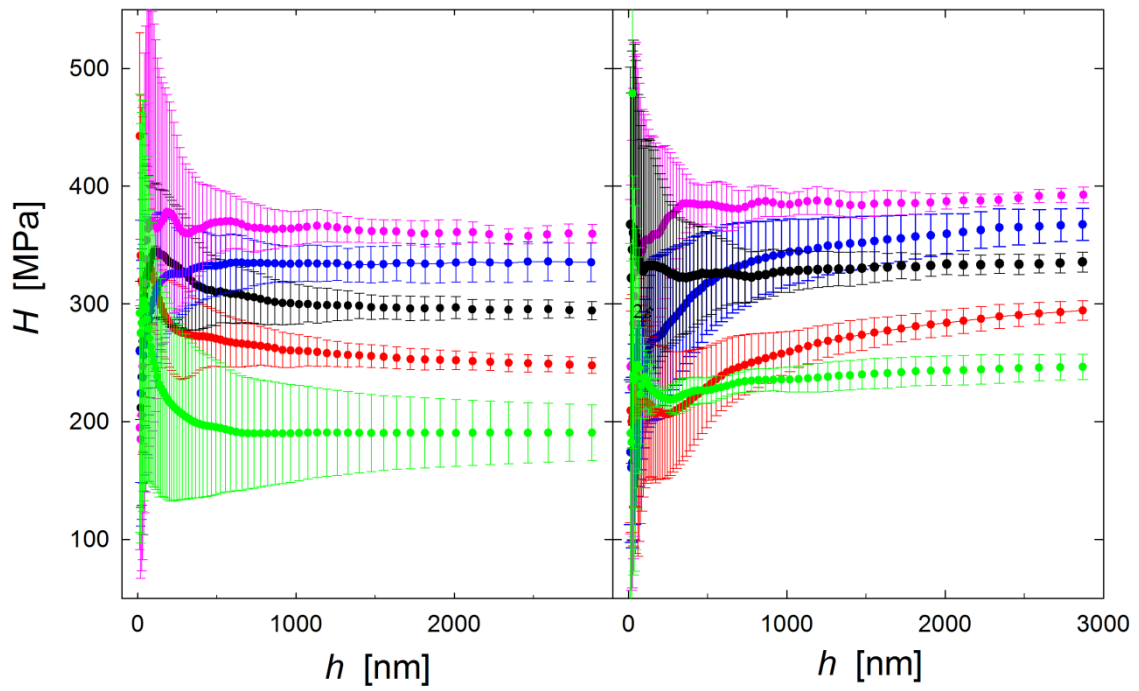


Fig. S5. Hardness,  $H$ , as a function of displacement into the surface,  $h$ , for: (left) PVA and (right) RGO-PVA, at different strain rates. From top to bottom:  $\dot{\varepsilon} = 0.15 \text{ s}^{-1}$ ,  $5 \times 10^{-2} \text{ s}^{-1}$ ,  $2.5 \times 10^{-2} \text{ s}^{-1}$ ,  $5 \times 10^{-3} \text{ s}^{-1}$  and  $5 \times 10^{-4} \text{ s}^{-1}$ . RH = 29%.



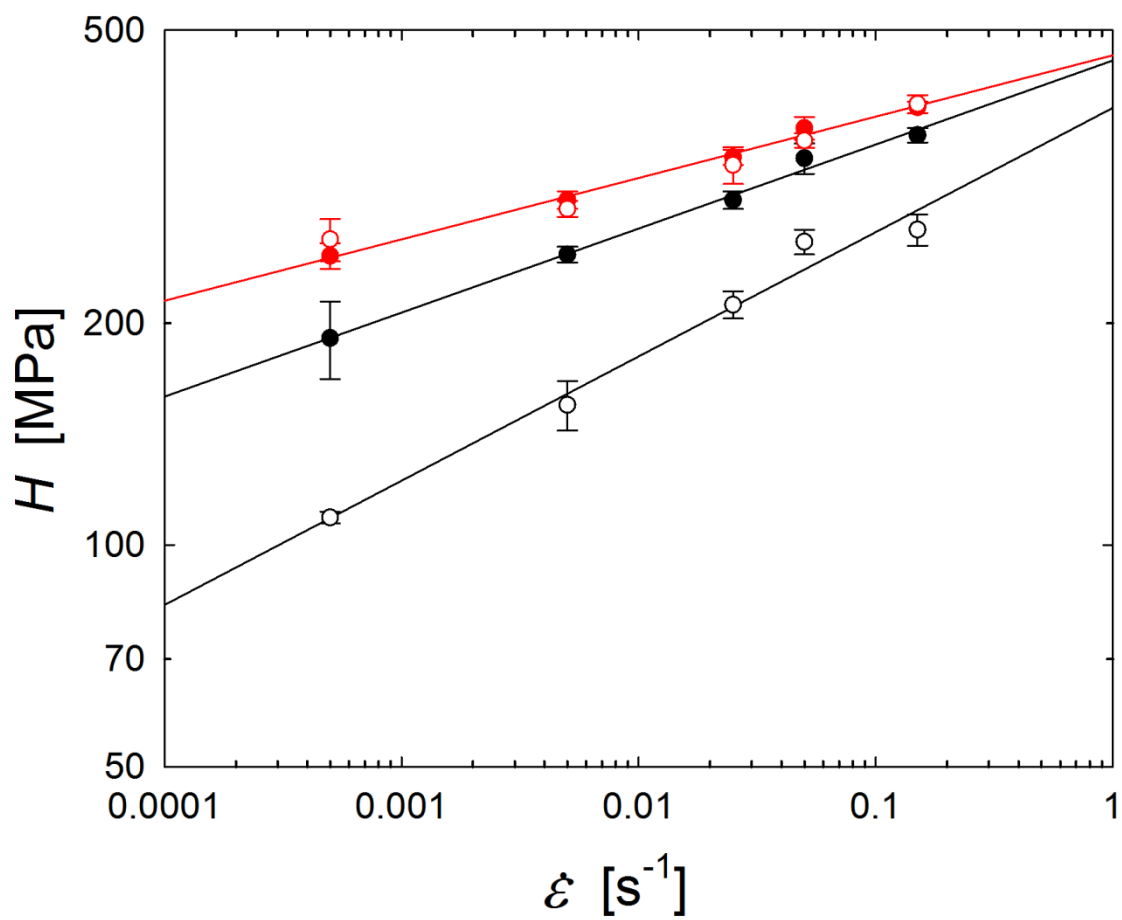


Fig. S6. Double logarithmic plot of  $H$  versus  $\dot{\epsilon}$  for: PVA at RH = (●) 29% and (○) 42%, and RGO-PVA at RH = (●) 29% and (○) 42%.

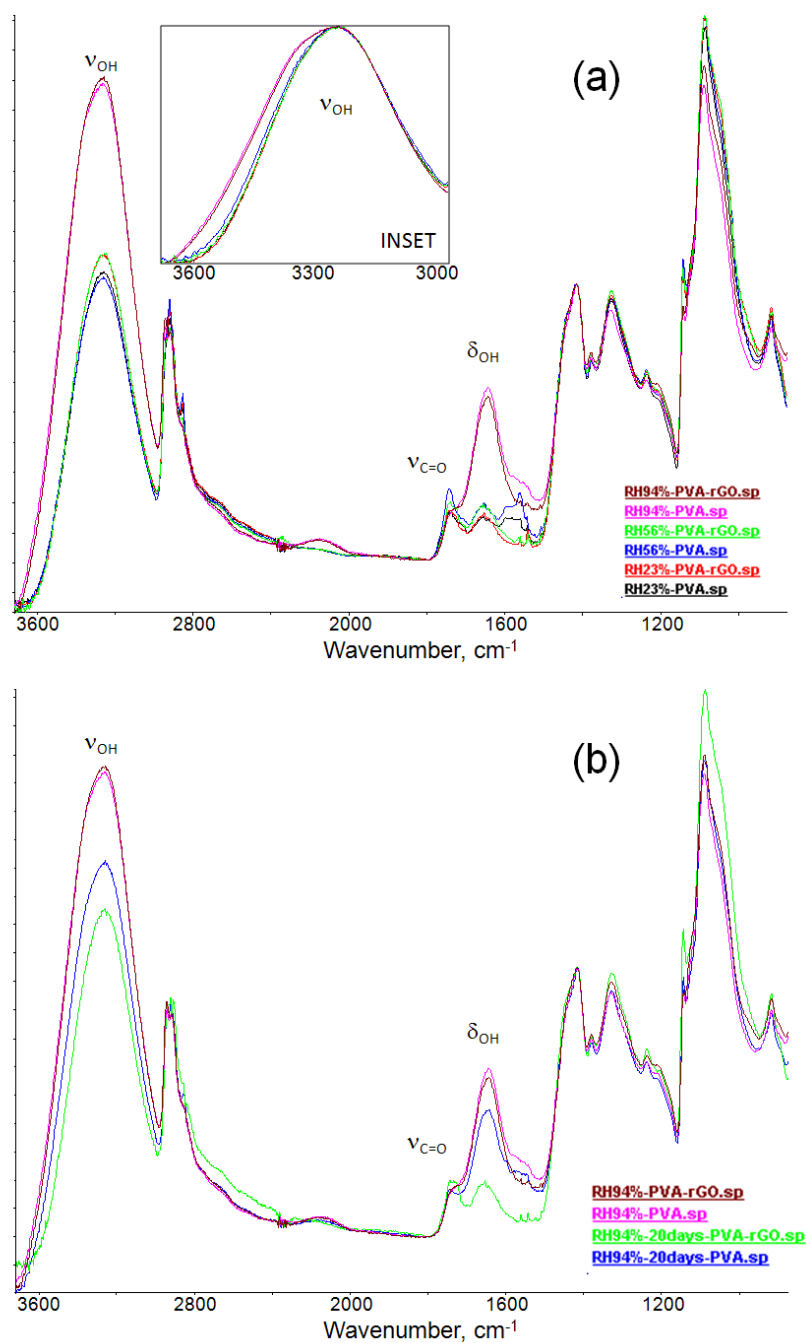


Fig. S7. FTIR spectra of (a) samples conditioned at different relative humidity: RH=23% (ambient), RH=56-59% (4h), RH=94% (4 days), and (b) comparison between spectra of RH=94% (4 days) and the same samples after 20 days storage in sealed Eppendorf vials at RT. All measurements made in open laboratory with RH=23-28%. Spectra normalized between 1400 and 1800  $\text{cm}^{-1}$ . Inset in (a) corresponds to the spectra normalized to maximum peak intensity of the  $\nu_{\text{OH}}$  region showing small variations in bandshape and bandwidth.

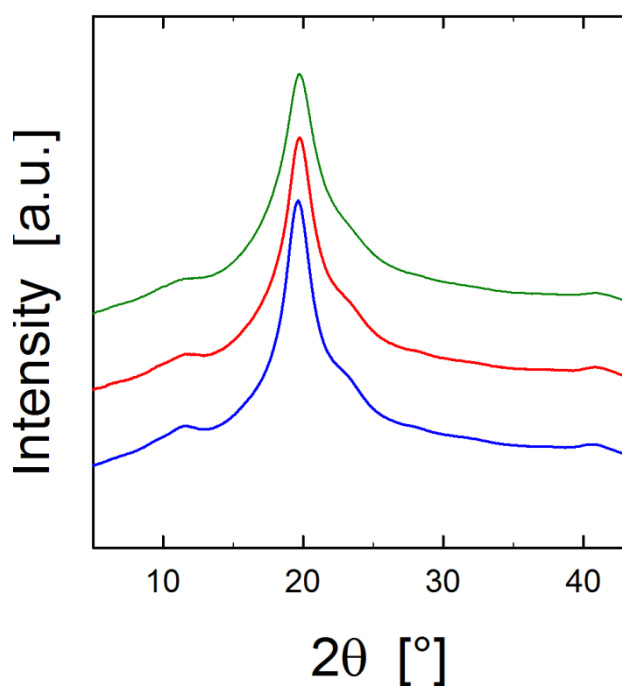


Fig. S8. WAXS profiles as a function of diffraction angle,  $2\theta$ , for PVA (blue line), RGO-PVA (red line) and GO-PVA (green line). RH = 31%.

#### References.

- 1 W. S. Hummers Jr., R. E. Offeman, *J. Am. Chem. Soc.* 1958, **80**, 1339–1339.
- 2 H. J. Salavagione, M. A. Gómez and G. Martínez, *Macromolecules* 2009, **42**, 6331–6334.
- 3 Y. Wang, H. Ono, A. Ikeda, N. Hori, A. Takemura, T. Yamada, T. Tsukatani, *Polymer*, 2006, **47**, 7827–7834.
- 4 J. P. Rourke, P. A. Pandey, J. J. Moore, M. Bates, I. A. Kinloch, R. J. Young, N. R. Wilson, *Angew. Chem. Int. Ed.*, 2011, **50**, 3173–3177.
- 5 V. R. Coluci, D. S. T. Martinez, J. G. Honório, A. F. de Faria, D. A. Morales, M. S. Skaf, O. L. Alves, G. A. Umbuzeiro, *J. Phys. Chem. C.*, 2014, **118**, 2187-2193.

- 6 H. R. Thomas, S. P. Day, W. E. Woodruff, C. Vallés, R. J. Young, I. A. Kinloch, G. W. Morley, J. V. Hanna, N. R. Wilson, J. P. Rourke, *Chem. Mater.*, 2013, **25**, 3580–3588.
- 7 W. C. Oliver, G. M. Pharr, *J. Mater. Res.*, 1992, **7**, 1564–1583.
- 8 J. B. Pethica, W. C. Oliver, *Mater. Res. Soc. Symp. Proc.*, 1989, **130**, 13–23.
- 9 C. C. White, M. R. Vanlandingham, P. L. Drzal, N. K. Chang, S. H. Chang, *J. Polym. Sci. B: Polym. Phys.*, 2005, **43**, 1812–1824.
- 10 E. G. Herbert, W. C. Oliver, G. M. Pharr, *J. Phys. D: Appl. Phys.*, 2008, **41**, 74021–74029.
- 11 G. M. Odegard, T. S. Gates, H. M. Herring, *Exp. Mech.*, 2005, **45**, 130–136.
- 12 J. L. Hay, P. Agee, E. Herbert. *Exp. Tech.*, 2010, **34(3)**, 86–94.
- 13 W. J. Wright, A. R. Maloney, W. D. Nix. *Int. J. Surf. Sci. Eng.*, 2007, **1(2/3)**, 274–292.
- 14 A. C. Fischer-Cripps, *Nanoindentation*, 2nd ed., Springer-Verlag: New York 2005.
- 15 W. J. Wright, W. D. Nix, *J. Mater. Res.*, 2009, **24(3)**, 863–871